

Article

Study on the Influence of Mining Stress on the Sustainable Utilization of Floor Roadway in Qinan Coal Mine

Yiqi Chen, Huaidong Liu, Changyou Liu *  and Shibao Liu

School of Mines, China University of Mining and Technology, Xuzhou 221116, China; yqchen@cumt.edu.cn (Y.C.); liuhuaidong@cumt.edu.cn (H.L.); cumtlsx@cumt.edu.cn (S.L.)

* Correspondence: znky2019@cumt.edu.cn

Abstract: Aiming at the problem of large deformations and difficult maintenance of cross-mining floor roadways, taking the track transportation roadway of the cross-mining east wing floor in Qinan Coal Mine as the engineering background, the stress field distribution of mining stress in floor strata and surrounding rock of floor roadway during the cross-mining process of the working face is studied by combining theoretical analysis with numerical simulation. The results show that the influence of mining stress on the vertical stress of floor strata is reflected in the stress-increasing area in front of the coal wall and the stress-decreasing area in the rear of the coal wall. With the increase in the depth of the floor strata, the peak value of the vertical stress gradually decreases, and the distance from the peak value of the vertical stress to the coal wall and the influence range of the vertical stress gradually increases. When the width of the coal pillar is greater than the influence range of advance abutment pressure of the working face, the development speed of the plastic zone is slow. When the roadway is located in the influence range of advance abutment pressure, the plastic zone of the roadway's surrounding rock develops rapidly. When the working face crosses the floor roadway more than 10 m, the depth of the plastic zone of the surrounding rock of the roadway is no longer increased; the siltstone above the roadway is the key layer of fracturing, and the deformation of the roadway has been effectively improved after hydraulic fracturing. Through the analysis of numerical simulation results, the fracturing scheme has a significant effect on the stability control of the surrounding rock of the cross-mining floor roadway. This study has certain guiding significance for the maintenance and sustainable utilization of floor roadways in the cross-mining process, which is conducive to ensuring the sustainable mining of underground coal and the safety of personnel and equipment and is of great significance to the sustainable development of the coal mining industry.

Keywords: mining stress; floor roadway; sustainable utilization; hydraulic fracturing; theoretical analysis; numerical simulation



Citation: Chen, Y.; Liu, H.; Liu, C.; Liu, S. Study on the Influence of Mining Stress on the Sustainable Utilization of Floor Roadway in Qinan Coal Mine. *Sustainability* **2024**, *16*, 2905. <https://doi.org/10.3390/su16072905>

Academic Editor: Adam Smoliński

Received: 4 March 2024

Revised: 25 March 2024

Accepted: 27 March 2024

Published: 30 March 2024



Copyright: © 2024 by the authors. Licensee MDPI, Basel, Switzerland. This article is an open access article distributed under the terms and conditions of the Creative Commons Attribution (CC BY) license (<https://creativecommons.org/licenses/by/4.0/>).

1. Introduction

The distribution characteristics of mining stress in the bottom roadway play a crucial role in the study of underground mining. With the progress of the upper working face, the width of the protective coal pillar alongside the bottom slab roadway decreases, leading to significant changes in the stress conditions of the bottom slab roadway. Consequently, the deformation and damage levels of the peripheral rock surrounding the roadway undergo a substantial increase. Therefore, understanding the propagation behavior of mining-induced stress in the rock layer of the bottom plate during cross-mining, elucidating the stress evolution patterns of the bottom plate roadway, and comprehending the mechanism that destabilizes the bottom plate roadway are crucial challenges in effectively managing the deformation of the surrounding rock in the bottom plate roadway [1]. It also has a certain guiding significance for the maintenance and sustainable utilization of the bottom roadway to better guarantee the sustainable mining of underground coal.

Numerous scholars, both domestically and internationally, have undertaken research concerning the distribution and propagation of mining-induced stress in the underlying rock stratum, as well as the destabilization mechanism of cross-mining roadways. Zhang Hualei et al. considered the quarry floor as a semi-infinite body and divided the stress field induced by mining into two components—the initial stress field of the rock and the additional stress field—and derived a criterion for the destruction of the floor [2,3]. Huang Qisong et al. employed the stiffness matrix solution method for the laminar elastic plane problem and developed an analytical calculation model that incorporates the impact of various rock deformation parameters on the transfer of mining-induced stress in the floor rock formation [4]. Ti Zhengyi et al. derived a formula for calculating the depth of mining-induced damage on the bottom plate using fracture mechanics and the double shear strength theory [5]. Zhu L et al. studied the influence of various factors on the deformation of the floor. It is considered that the influencing factors of the floor uplift are large buried depth, long duration of dynamic pressure, unique characteristics of the surrounding rock, and insufficient support strength [6,7]. Zhai Xinxian et al. proposed the concept of the payload coefficient to summarize the quantitative relationship between the deformation of the perimeter rock of the bottom roadway and the payload coefficient during the cross-mining period [8]. Wang Pengpeng et al. utilized the 3DEC 5.2 software to investigate the impact of different pressurization steps on the development of the stress field and plastic zone within the rock layer at the base of the working face [9]. He Fulian et al. conducted a study on the mechanism of asymmetric floor bulge in roadways. They concluded that the primary factors contributing to the main roadway floor bulge are plateau rock stress, surrounding rock stress, water action, and support strength [10]. Liu Weitao et al. derived the far-field stress solution and the elastic solution for stress and deformation of the roadway surroundings under the influence of mining in the bottom slab roadway based on elastic theory [11]. Skrzypkowski et al. believe that more attention should be paid to the discontinuous deformation of fault forms, which has an important impact on the change of excavation protection scheme [12]. Some scholars conducted a study on the morphology of the displacement field and stress field distribution in the peripheral rock of a high-level stress floor roadway during the cross-mining process and pointed out that the shoulder corner of the roadway is a key area that affects the stability of the surrounding rock [13–15]. In order to minimize the impact of mining stresses on the roadway, some scholars have proposed cross-mining pressure relief technical schemes such as pre-excavation pressure relief mining [16,17], borehole loose blasting [18], and insufficient mining [19]. However, traditional decompression technology has several disadvantages, such as difficulties in ensuring the effectiveness of decompression, complex construction processes, and lengthy construction periods. The hydraulic fracturing-based pressure unloading control technology for trans-mining roadways is considered to be more convenient and flexible in terms of time and space compared to traditional pressure unloading methods. This technology represents a significant advancement in the field of pressure unloading and is recognized as one of the key directions for its development.

The deformation of cross-mining roadways mainly stems from the deteriorating stress environment of peripheral rocks induced by mining stress, which has a great influence on the sustainable utilization of the subgrade roadway [20]. However, there is limited research on the dynamic evolution characteristics of stress fields in peripheral rocks of subgrade roadways during cross-mining. In particular, the employment of hydraulic fracturing and decompression technology to mitigate the impact of mining stress on subgrade roadways remains an area that requires further investigation. Based on previous research, this paper takes the Qinan Coal Mine through mining east wing bottom plate rail transportation alley as the engineering background. FLAC3D is employed to examine and analyze the stress distribution characteristics and evolutionary patterns of the surrounding rocks in the bottom plate alley during trans-mining. Furthermore, the extent of damage to the surrounding rocks in the bottom plate alley under various coal pillar widths in the protective alley is investigated. A control technique involving hydraulic fracturing decompression

is proposed, and the impact of fracturing parameters on the decompression effectiveness is analyzed. Additionally, the influence of fracturing parameters on the decompression effect is explored, which provides a basis for controlling the surrounding rock in the bottom slab road.

2. Engineering Background

The 31 mining area of Qinan Coal Mine of Huabei Mining Co., Ltd. is located in the eastern part of the well field. The mine shaft is positioned on the first level of the 3_2 coal seam. The east wing rail transport roadway is arranged in the sandstone layer with a thickness of 18 m under the 3_2 coal seam. It is 40 m away from the coal seam floor of the 313 working face in the 31 mining area. The angle with the length direction of the working face is 19° , and the intersection length with the working face is 267 m. The width of the protective coal pillar is 80 m between the design and the stop mining position of the working face. In order to improve the recovery rate of coal resources, it is planned to cross the main roadway, as shown in Figure 1. The length of the main roadway located on the inner side of the expected receiving line is 92 m, and the horizontal distance from the expected receiving line is 0–29 m.

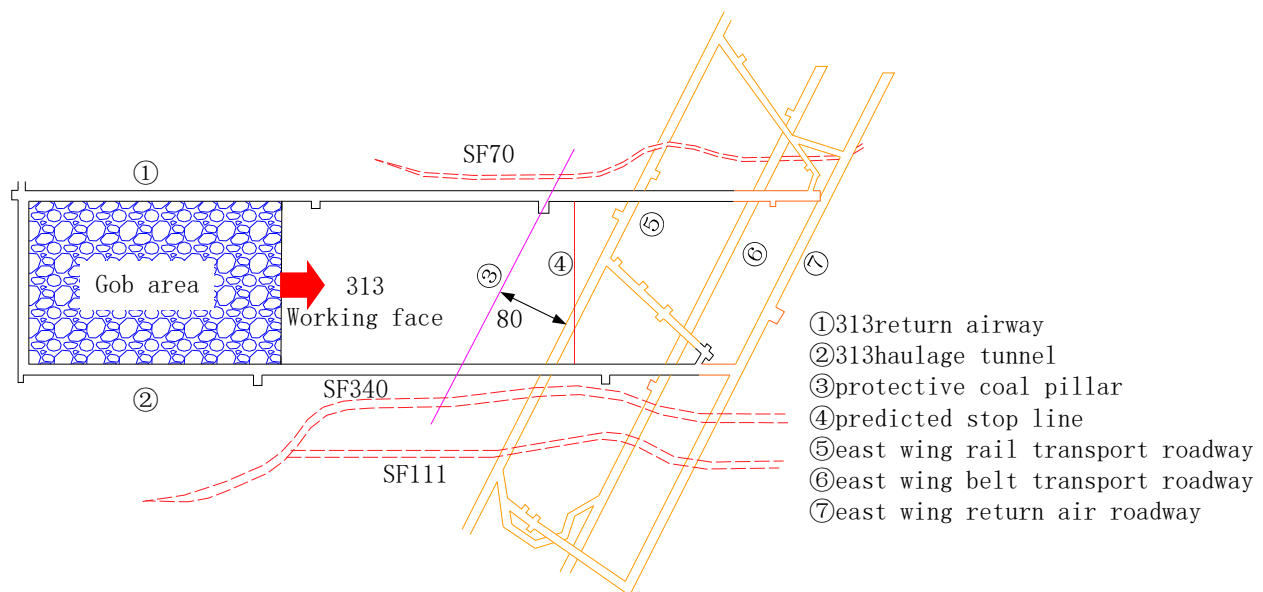


Figure 1. Layout diagram of 313 working face in Qinan Coal Mine.

The 313 working face mines the 3_2 coal seam, with a coal thickness of 1.3–3.5 m, an average of 2.8 m; the buried depth is 400–540 m, with an average of 470 m. The dip angle of the coal seam is 6° – 15° , with an average of 12° . The average buried depth of the coal seam from 80 m in front of the coal pillar to the stop line is 520 m, and the average dip angle is 7.9° . The roof lithology of the coal seam is mainly mudstone and siltstone, and the floor lithology is mainly mudstone. The rock mass parameters of different strata of coal seam roof and floor are shown in Table 1.

The 313 working face adopts the inclined longwall comprehensive mechanized coal mining method, with an average daily advance of 2–4 m; the whole caving method is used to deal with the goaf.

The section of the floor roadway is a semi-circular arch with a net width of 5 m and a net height of 4 m. The roadway initially implemented a high-strength support. The high-strength bolt specification is $\phi 20 \times L2800$ mm, the row spacing is 800×800 mm, the anchor cable specification is YMS17.8/6500 mm, and the row spacing is 1600×1600 mm. The '3-0-3' arrangement is adopted. In order to reduce the risk of deformation and failure of roadway surrounding rock under the influence of mining during the cross-mining period, secondary strengthening support was carried out for the roadway. The $\phi 20 \times L2800$ mm

high-strength bolt was used with 4 m of M steel belt combined support, and the row spacing between the bolts was 800×800 mm. At the same time, the surrounding rock of the roadway was modified by grouting. The grouting bolt specification was $\phi 20 \times L2050$ mm, the row spacing was 1600×1600 mm, the slurry water–cement ratio was 0.7:1, and the grouting pressure was greater than 2 MPa.

Table 1. Rock mass parameters of coal seam and roof and floor strata in 313 working face of Qinan Coal Mine.

| Rock | Thickness/m | Densities/Kg·m ⁻³ | Modulus of Elasticity/GPa | Poisson's Ratio | Cohesion/MPa | Angle of Internal Friction/° | Tensile Strength/MPa |
|-------------|-------------|------------------------------|---------------------------|-----------------|--------------|------------------------------|----------------------|
| Mudstone-3 | 3.5 | 2550 | 3.34 | 0.29 | 2.24 | 33.10 | 0.83 |
| Siltstone-1 | 6.2 | 2570 | 5.15 | 0.20 | 3.72 | 35.86 | 1.42 |
| Mudstone-2 | 6.6 | 2550 | 3.34 | 0.26 | 2.24 | 33.10 | 0.83 |
| Sandstone-1 | 3.7 | 2730 | 6.67 | 0.16 | 5.18 | 36.73 | 3.02 |
| Mudstone-1 | 2.2 | 2550 | 2.50 | 0.26 | 2.42 | 26.93 | 0.52 |
| 32mine | 2.8 | 1490 | 1.94 | 0.32 | 0.65 | 24.60 | 0.12 |
| mudstone-1 | 2.8 | 2590 | 4.35 | 0.26 | 1.34 | 27.49 | 0.50 |
| siltstone-1 | 1.8 | 2630 | 6.63 | 0.20 | 2.84 | 36.30 | 1.45 |
| mudstone-2 | 2.4 | 2590 | 4.35 | 0.26 | 2.17 | 34.09 | 0.74 |
| sandstone-1 | 5.7 | 2590 | 8.65 | 0.16 | 5.09 | 39.90 | 2.34 |
| mudstone-3 | 5.8 | 2590 | 4.35 | 0.26 | 2.17 | 34.09 | 0.74 |
| siltstone-2 | 12 | 2630 | 6.63 | 0.20 | 2.84 | 36.30 | 1.45 |
| mudstone-2 | 18 | 2590 | 8.65 | 0.16 | 5.09 | 39.90 | 2.34 |

3. Propagation Law of Mining Stress in Floor Strata

3.1. Theoretical Analysis of the Propagation Law of Mining Stress in Floor Strata

3.1.1. Solution of Mining-Induced Stress

After the mining of the coal seam in the working face, the weight of the overlying strata in the goaf is transferred to the surrounding rock mass, and the advanced abutment pressure is formed in the coal seam in front of the working face. The coal body close to the working face is destroyed due to the abutment pressure exceeding its ultimate strength, forming a plastic zone, and its bearing capacity is reduced so that the high stress is transferred to the deep part of the coal body. Therefore, a certain range of stress reduction zone and stress increase zone are formed in the coal seam in front of the working face. In the goaf behind the working face, with the caving and sinking of the overlying strata, the fallen gangue is gradually compacted, and its bearing pressure can gradually recover to the original rock stress. The distribution of mining stress in the coal seam is shown in Figure 2.

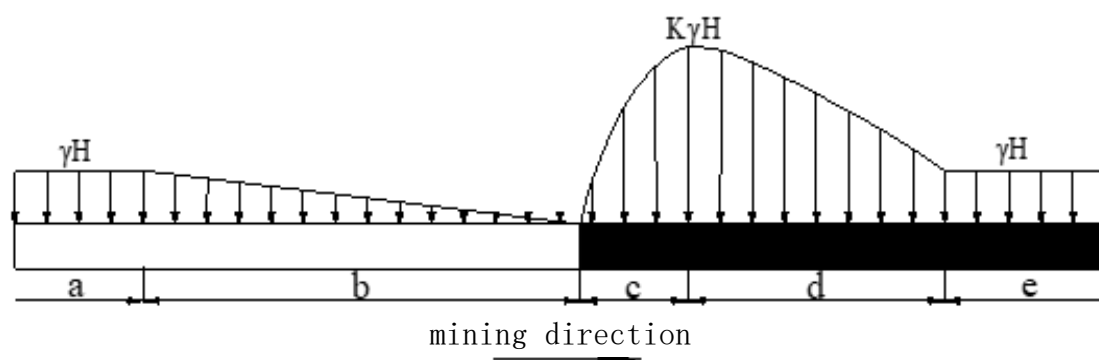


Figure 2. Coal seam mining stress distribution. (a) compacted area; (b) gradual compaction zone; (c) limit equilibrium region; (d) elastic pressurization zone; (e) original rock stress zone.

After the coal seam is mined, the floor strata can be approximately regarded as a semi-infinite body, ignoring the lateral abutment pressure formed by mining, and the vertical section along the advancing direction of the working face can be treated as plane

strain. In order to facilitate the theoretical calculation and analysis, the mining stress is linearly simplified, as shown in Figure 3.

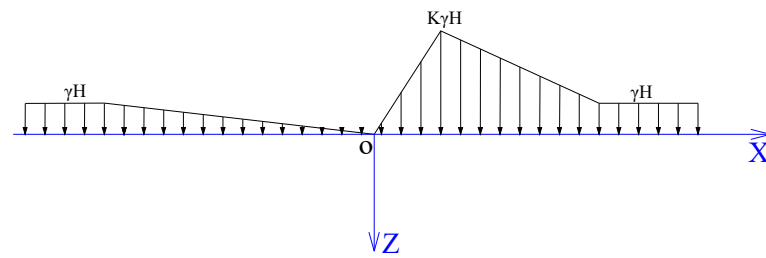


Figure 3. Simplified diagram of mining stress in coal seam.

According to the principle of stress superposition, the mining stress in the coal seam can be regarded as the superposition of the abutment pressure and the original rock stress, as shown in Figure 4. To study the propagation law of mining stress in floor strata, the focus is on the distribution of abutment pressure in floor strata.

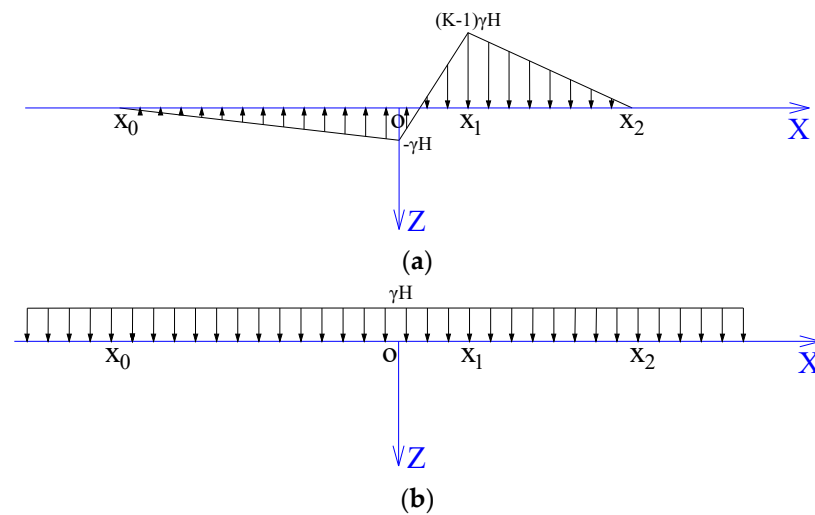


Figure 4. Mining stress decomposition diagram: (a) abutment pressure; (b) stress in original rock.

In Figure 4, K is the maximum stress concentration factor. The working face is located at the origin. The left side of the origin is the goaf area, and the right side of the origin is the unmined area. $(x_0, 0)$ is the coordinate of the position where the goaf just restores to the original rock stress. Point $(x_1, 0)$ is the peak coordinate of the advance abutment pressure of the coal seam, and point $(x_2, 0)$ is the coordinate of the influence range of the advance abutment pressure of the coal seam.

The distribution set of abutment pressure shown in Figure 4 is expressed by piecewise function, and the mathematical expression is shown in Equation (1).

$$\begin{cases} q_0 = \frac{\gamma H}{x_0} \xi - \gamma H & x_0 < \xi < 0 \\ q_1 = \frac{K\gamma H}{x_1} \xi - \gamma H & 0 < \xi < x_1 \\ q_2 = -\frac{(K-1)\gamma H}{x_2-x_1} \xi + \frac{(K-1)\gamma H}{x_2-x_1} x_2 & x_1 < \xi < x_2 \end{cases} \quad (1)$$

In the formula, H is the buried depth of the coal seam in the working face, 520 m.

3.1.2. Effect of Abutment Pressure on Floor Strata

From elastic mechanics [21], it is known that the stress component expression of any point in a half-plane with a vertical concentrated force F at the boundary in the Cartesian coordinate system shown in Figure 5 is

$$\begin{cases} \sigma_z = \frac{2F}{\pi} \frac{z^3}{(x^2+z^2)^2} \\ \sigma_x = \frac{2F}{\pi} \frac{zx^2}{(x^2+z^2)^2} \\ \tau_{xz} = -\frac{2F}{\pi} \frac{z^2x}{(x^2+z^2)^2} \end{cases} \quad (2)$$

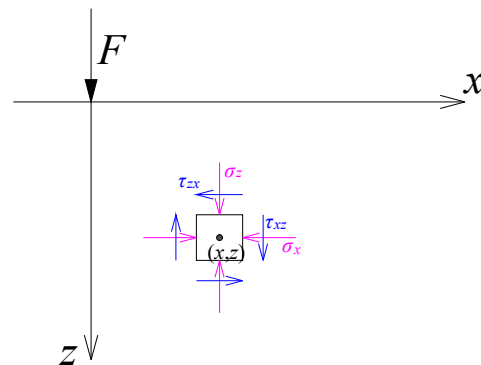


Figure 5. The hemihedron is subjected to a concentrated force on the boundary.

If the boundary of the half-plane is subjected to a vertical distribution force, the distribution force concentration at the distance from the origin ‘ ξ ’ is p , as shown in Figure 6. Take a small length ‘ $d\xi$ ’ at ‘ ξ ’, and the force in the range of ‘ $d\xi$ ’ can be regarded as a small concentrated force dF , ‘ $dF = pd\xi$ ’. The component expression of the stress caused by the concentrated force at any point in the half plane in the rectangular coordinate system is

$$d\sigma_z = \frac{2pd\xi}{\pi} \frac{z^3}{[z^2 + (x - \xi)^2]^2} \quad (3)$$

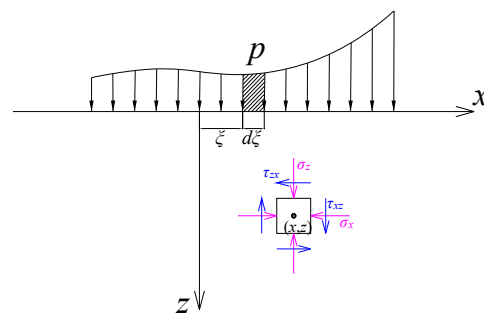


Figure 6. The distributed force on the boundary of the hemishedron.

By integrating the Formula (3) in the distribution range of the distributed force, the stress caused by the whole distributed force at any point in the semi-infinite body can be solved.

According to the above analysis, it can be seen that the σ_{z0} at the point (x, z) of the q_0 section in the abutment pressure is

$$\begin{aligned} \sigma_{z0} &= \frac{2}{\pi} \int_{x_0}^0 \frac{(\frac{\gamma H}{x_0} \xi - \gamma H) z^3 d\xi}{[z^2 + (x - \xi)^2]^2} = \frac{2\gamma H}{\pi x_0} \frac{(\xi - x_0) z^3 d\xi}{[z^2 + (x - \xi)^2]^2} \\ &= (-\frac{\gamma H}{\pi x_0} x + \frac{\gamma H}{\pi}) (\arctan \frac{x}{z} - \arctan \frac{x-x_0}{z}) + \frac{\gamma H}{\pi} \frac{xz}{x^2+z^2} \end{aligned} \quad (4)$$

The σ_{z1} of the q_1 section at point (x, z) in the abutment pressure is

$$\begin{aligned}\sigma_{z1} &= \frac{2}{\pi} \int_0^{x_1} \frac{\left(\frac{K\gamma H}{x_1} \xi - \gamma H\right) z^3 d\xi}{[z^2 + (x - \xi)^2]^2} = \frac{2\gamma H}{\pi x_1} \int_0^{x_1} \frac{(K\xi - x_1) z^3 d\xi}{[z^2 + (x - \xi)^2]^2} \\ &= \left(-\frac{K\gamma H}{\pi x_1} x + \frac{\gamma H}{\pi}\right) \left(\arctan \frac{x - x_1}{z} - \arctan \frac{x}{z}\right) \\ &\quad - \frac{\gamma H}{\pi x_1} z \left(\frac{Kx^2 - (K+1)xx_1 + Kz^2 + x_1^2}{(x - x_1)^2 + z^2} - \frac{Kx^2 + Kz^2 - xx_1}{x^2 + z^2}\right)\end{aligned}\quad (5)$$

The σ_{z2} of the q_2 section at point (x, z) in the abutment pressure is

$$\begin{aligned}\sigma_{z2} &= \frac{2}{\pi} \int_{x_1}^{x_2} \frac{\left[\frac{(1-K)\gamma H}{x_2 - x_1} \xi + \frac{x_2(K-1)\gamma H}{x_2 - x_1}\right] z^3 d\xi}{[z^2 + (x - \xi)^2]^2} \\ &= \frac{2(1-K)\gamma H}{\pi(x_2 - x_1)} \int_{x_1}^{x_2} \frac{(\xi - x_2) z^3 d\xi}{[z^2 + (x - \xi)^2]^2} \\ &= \left[-\frac{(1-K)\gamma H}{\pi(x_2 - x_1)}(x - x_2)\right] \left(\arctan \frac{x - x_2}{z} - \arctan \frac{x - x_1}{z}\right) \\ &\quad - \frac{(1-K)\gamma H}{\pi(x_2 - x_1)} z \left[1 - \frac{x^2 + z^2 - xx_1 - xx_2 + x_1 x_2}{(x - x_1)^2 + z^2}\right]\end{aligned}\quad (6)$$

According to the principle of stress superposition, the bearing pressure of any point in the floor rock layer is equal to the sum of the stresses caused by the load q_0 , q_1 , and q_2 at this point.

$$\sigma'_z = \sigma_{z0} + \sigma_{z1} + \sigma_{z2}\quad (7)$$

According to the conservation of energy, mining activities will not cause an increase or decrease in the total stress in the formation but only make the stress transfer, forming a certain range of stress increase area and stress decrease area, but the total stress is unchanged. Therefore, the total abutment pressure should be 0; that is, the sum of mining stress in the coal seam is equal to the sum of the original rock stress. Formula (8) can be obtained accordingly.

$$\frac{1}{2}K\gamma Hx_1 + \frac{1}{2}(K+1)\gamma H(x_2 - x_1) - \frac{1}{2}\gamma Hx_0 = \gamma H(x_2 - x_0)\quad (8)$$

According to Formula (8), the relationship between the length of the gradually compacted zone in the goaf and the peak value of the advance abutment pressure and the distance from the influence range to the coal wall can be solved.

$$x_0 = (1 - K)x_2 + x_1\quad (9)$$

According to the observation of mine pressure in the Qinan Coal Mine, the influence range of advance abutment pressure is $x_2 = 30$ m. Jiang Jinqun et al. pointed out that the distance between the peak abutment pressure and the coal wall in the longwall face of coal mines in China is generally 2~3.5 times the mining height [20]. The coal seam mining height of 313 working face in Qinan Coal Mine is 2.8 m, so it can be obtained that the peak abutment pressure of the coal seam is about 10 m away from the coal wall, that is, $x_1 = 10$ m. A.H. Wilson [7] proposed the stress concentration factor at the limit equilibrium point of the coal wall; that is, the maximum stress concentration factor is

$$K = k + \frac{\sigma_0}{\gamma H}\quad (10)$$

In the formula, $k = (1 + \sin \varphi) / (1 - \sin \varphi)$, $\varphi = 24.60^\circ$, $\sigma_0 = 1.23$ MPa. So, $k = 2.43$, $K = 2.52$.

Taking x_1 , x_2 , and K into Formula (9), we can conclude that the distance x_0 is -35.6 m. Then, taking x_0 , x_1 , x_2 , and K into Formula (7), using Matlab 2022a and Origin2021a software to calculate and draw the stress curve and contour map, we can obtain Figure 7.

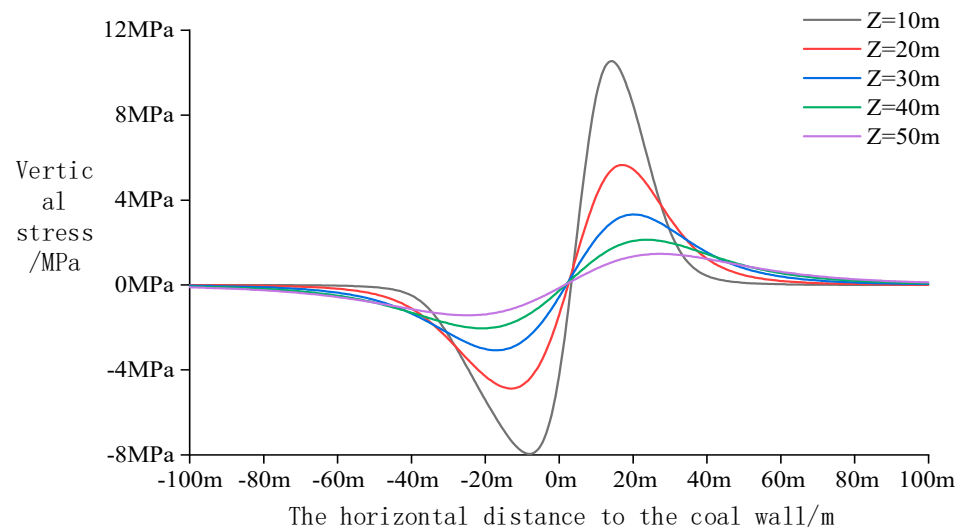


Figure 7. Additional vertical stress curve of floor strata mining.

From the graph, we can see that the vertical stress caused by abutment pressure in the floor strata is mainly compressive stress in front of the coal wall. In the horizontal direction, with the increase in the distance to the coal wall, the vertical stress first increases gradually, then decreases gradually after reaching the peak stress position, and finally returns to 0. In the vertical direction, with the increase in the depth of the floor rock layer, the peak stress gradually decreases, especially in the shallow part of the floor rock layer; the decrease in the peak stress is particularly significant. With the increase in depth, the distribution of vertical stress in the vertical and horizontal directions tends to be stable, the peak stress decreases gradually, the reduction rate of the peak stress decreases continuously, and the stress curve becomes more and more gentle, gradually approaching the '0 MPa horizontal line'. However, the influence range of vertical stress in the horizontal direction increases with the increase in depth.

3.1.3. Distribution of Mining-Induced Stress in Floor Strata

The stress caused by mining stress at any point of the floor is equal to the sum of the stress caused by the abutment pressure at this point and the original rock stress at this point, so,

$$\sigma_z = \sigma_{z0} + \sigma_{z1} + \sigma_{z2} + \gamma H \quad (11)$$

According to Formula (11), using Matlab and Origin software to solve the vertical stress of the floor strata from 100 m behind the coal wall to 100 m in front of the coal wall and the depth of 50 m, a contour map was drawn, as shown in Figure 8. With the increase in the depth of the floor rock, the stress concentration factor in the stress-increasing area in front of the coal wall gradually decreases, and the stress concentration factor in the stress-reducing area behind the coal wall gradually increases. With the increase in the depth of the floor rock layer, the contour density of the vertical stress concentration coefficient decreases continuously. Within 50 m of the floor strata, the influence range of vertical stress gradually increases with the depth of the floor, but the increase rate gradually decreases. When the depth is about 50 m, the influence range of vertical stress reaches the maximum, about 55 m in front of and behind the coal wall; as the depth continues to increase, the influence of vertical stress begins to decrease gradually.

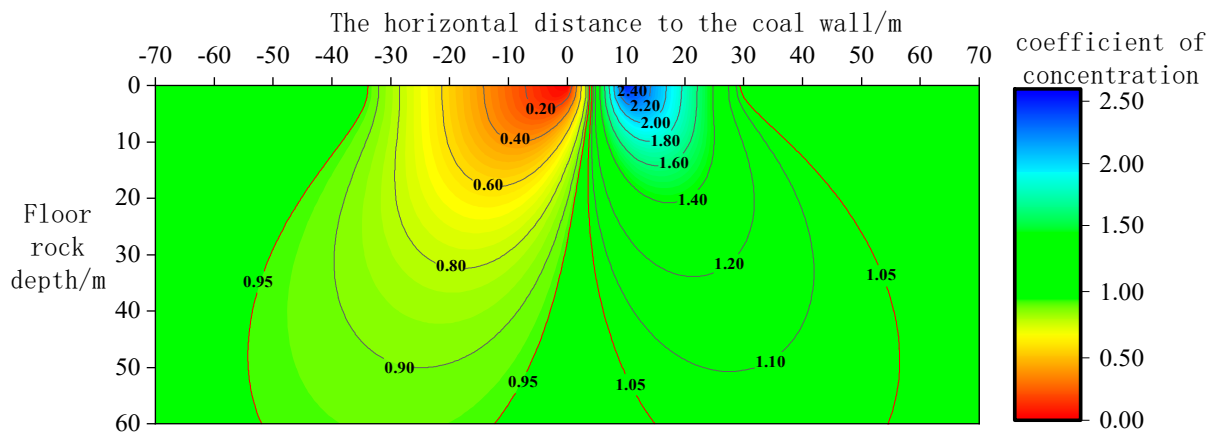


Figure 8. Contour map of vertical stress concentration factor.

3.2. Numerical Calculation and Analysis of Mining Stress Propagation in Floor Strata

In the previous section, the propagation law of mining-induced stress in floor strata is studied and analyzed. However, the theoretical calculation makes more assumptions and simplifications on the mechanical model. It is obviously not enough to rely solely on theoretical calculation. In this section, FLAC3D 5.2 software is used for numerical simulation research.

3.2.1. Model Set-Up

The model size is 400×246 (working face length) $\times 100$ m, the thickness of the coal seam is 2.8 m, the buried depth is 520 m, the average dip angle is 7.9° , and the influence of dip angle is ignored. The total thickness of the model floor rock is 75 m, and the vertical displacement is limited at the bottom. The total thickness of the roof strata of the model is 22.2 m, and the equivalent load of the overlying strata is 12.39 MPa. The horizontal displacement is limited before and after the model, left and right, as shown in Figure 9.

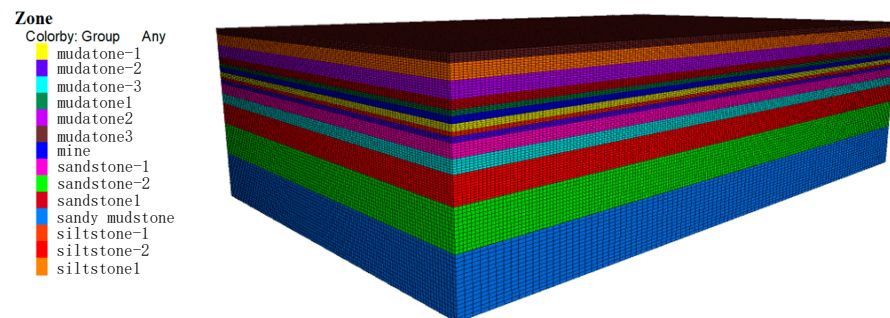


Figure 9. Three-dimensional numerical model.

In order to eliminate the influence of the boundary effect of the model, the advancing length of the simulated working face is 250 m, and 75 m coal pillars are left on both sides of the model. The calculation process uses the FISH function to mine the coal seam step by step, 2 m each time and cycle 500 steps.

3.2.2. Propagation Law of Mining-Induced Stress in Floor Strata

Along the advancing direction of the working face, the rock mass in the middle of the stope is selected as the research object. Six survey lines are arranged in the floor strata from 40 m behind the coal wall to 60 m in front of the working face, which are 0.70 m, 9.85 m, 20.50 m, 30.50 m, 41.00 m, and 50.00 m from the coal seam floor, respectively. Each survey line is 100 m long and consists of 51 measuring points. It is used to monitor the distribution

of vertical stress in different depth ranges of floor strata from 40 m behind the coal wall to 60 m in front of the coal wall when the working face advances 90 m, as shown in Figure 10.

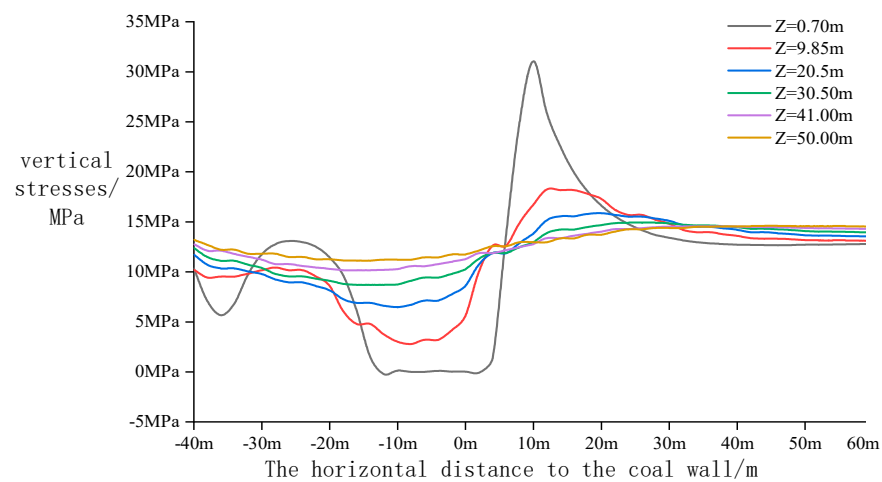


Figure 10. Vertical stress distribution curve of floor strata.

It can be seen from Figure 10 that the vertical stress of the floor rock stratum is similar to the theoretical calculation result. The influence of mining stress on the vertical stress of the floor rock stratum is in front of the coal wall, which is mainly reflected in the stress increase area. Behind the coal wall, it is mainly reflected in the stress reduction zone. With the increase in the depth of the floor strata, the peak value of the vertical stress gradually decreases, and the distance from the peak value of the vertical stress to the coal wall and the influence range of the vertical stress gradually increases. The stress curve is more and more gentle, and the stress curve obtained by theoretical calculation is more similar. Compared with the theoretical calculation, with the increase in depth, the peak value of vertical stress decreases faster, and the peak value of vertical stress at different depths of the floor rock layer is also smaller than that of theoretical calculation, but the variation law of vertical stress in horizontal and vertical directions is basically consistent with the theoretical calculation.

3.2.3. Floor Rock Failure under Mining Stress

The distribution law of the advanced abutment pressure in the floor strata of the working face is shown in Figure 11. If the influence boundary is 5% more than the original rock stress, the influence range of the advanced abutment pressure of the coal seam floor can reach 41.71 m in the vertical direction and 35.63 m in the horizontal direction. The floor of the roadway is 40 m away from the coal seam. Although the depth of the failure zone of the coal seam floor does not affect the surrounding rock of the roadway, the floor roadway is within the range of the influence depth of the advance abutment pressure, so it is bound to be affected by the mining stress in the process of cross mining.

The failure zone of the coal seam and its roof and floor strata is shown in Figure 12. From the figure, it can be seen that the maximum failure depth of floor strata is 18.5 m, and the failure zone develops to ‘mudstone-3’ strata. Through this process, it can be seen that the failure zone of the floor rock stratum does not necessarily develop gradually from the shallow to the deep. In this simulation, the soft rock strata above and below the hard rock stratum of the floor first fail and then develop to the hard rock stratum in the middle of the failure zone.

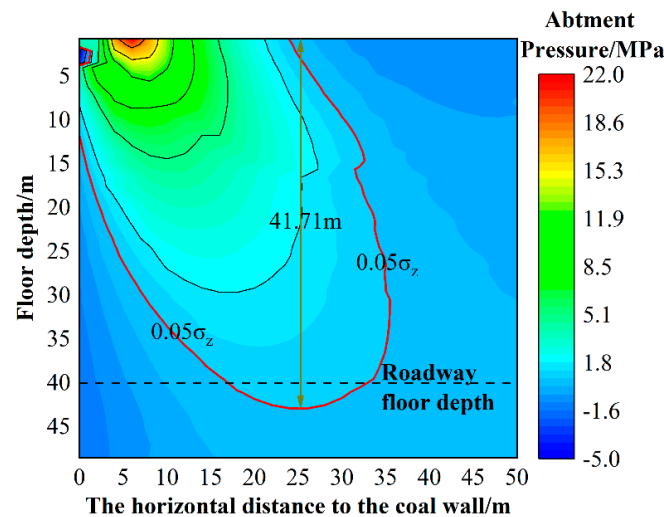


Figure 11. Distribution of leading abutment pressure in floor strata in working face.

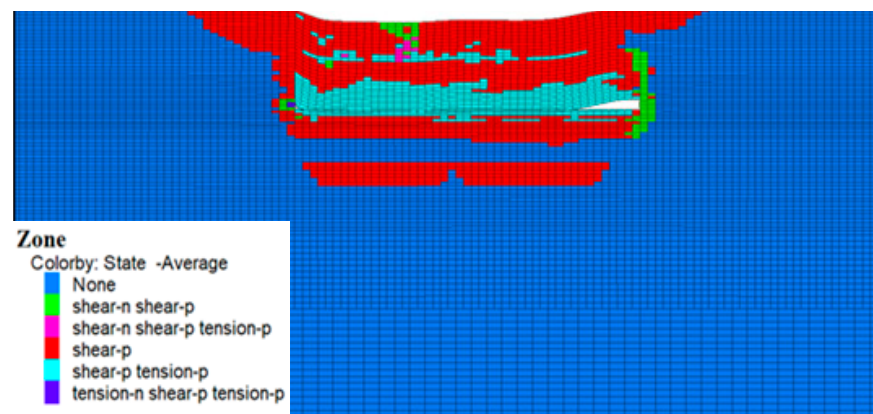


Figure 12. The failure area of the coal seam and its roof and floor strata.

4. Analysis of the Influence of Mining Stress on Floor Roadway

The deformation and failure of cross-mining dynamic pressure roadways are more serious than those of static pressure roadways, and its mechanism is more complex. The mining-induced stress formed by coal seam mining propagates to the deep floor, which makes the stress of the floor strata redistribute. The redistribution of the surrounding rock stress of the floor roadway is an important factor affecting the stability of the cross-mining roadway. Therefore, it is necessary to deeply analyze the influence of mining stress on the stress distribution of the roadway's surrounding rock and the deformation and failure mechanism of the roadway's surrounding rock under mining stress with the decrease in coal pillar width.

4.1. Theoretical Analysis of Stress Distribution of Roadway Surrounding Rock under the Influence of Mining Stress

Without considering the influence of mining stress on the floor roadway, ignoring the weight of rock in the influence range of the roadway, the vertical stress in this range is replaced by uniform stress, which is equal to the vertical stress value of the center depth of the roadway, as shown in Figure 13. In view of the close distance between Luling Coal Mine and Qinan Coal Mine, about 20 km, and the similar geological conditions of the two mines, the ratio of the maximum and minimum horizontal principal stresses to the vertical stress is constant according to the in situ stress measurement results of Luling Coal Mine, $\lambda_1 = 1.64$, $\lambda_2 = 0.67$ [22]. Therefore, the three principal stresses of the original rock

stress around the roadway are simplified as uniform stress, and the stress distribution around the roadway can be regarded as a plane strain circular hole problem [19].

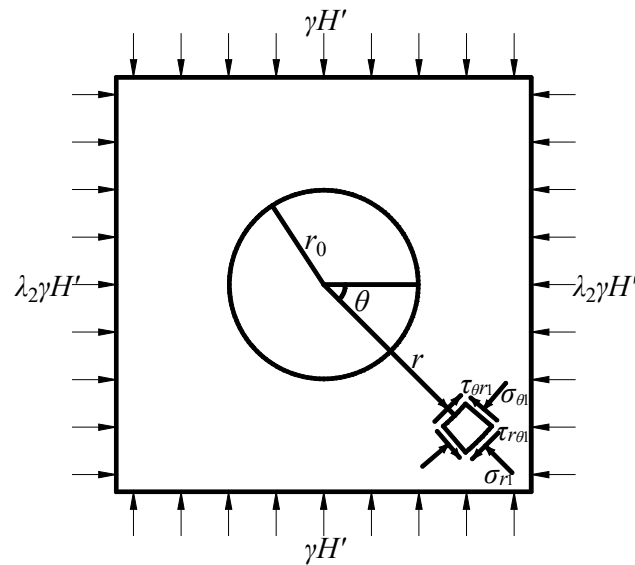


Figure 13. Stress distribution around circular static pressure roadway.

In the figure, r_0 is the radius of the circular roadway section; r is the distance from the micro-unit to the center of the roadway; θ is the radiation angle of the micro-element in the polar coordinate system; H' is the buried depth of roadway center, 558.5 m; λ_2 is the lateral pressure coefficient of the roadway surrounding rock. According to the analysis of the previous chapter, $\lambda_2 = 0.67$; the σ_{r1} is the circumferential stress of the micro-element; the $\sigma_{\theta1}$ is the radial stress of the micro-element; $\tau_{r\theta1}$ and $\tau_{\theta r1}$ are the tangential stress on the micro-element. According to the reciprocal theorem of shear stress, $\tau_{r\theta1} = -\tau_{\theta r1}$. According to the Kiers solution of elastic mechanics, in the coordinate system shown in Figure 13, the stress state of any point in the surrounding rock of the static pressure roadway can be expressed by the Formula (12).

$$\begin{cases} \sigma_{r1} = \frac{\gamma H'}{2} \left[(1 + \lambda) \left(1 - \frac{r_0^2}{r^2} \right) - (1 - \lambda) \left(1 - \frac{4r_0^2}{r^2} + \frac{3r_0^4}{r^4} \right) \cos 2\theta \right] \\ \sigma_{\theta1} = \frac{\gamma H'}{2} \left[(1 + \lambda) \left(1 + \frac{r_0^2}{r^2} \right) + (1 - \lambda) \left(1 + \frac{3r_0^4}{r^4} \right) \cos 2\theta \right] \\ \tau_{r\theta1} = -\frac{\gamma H'}{2} (1 - \lambda) \left(1 + \frac{2r_0^2}{r^2} - \frac{3r_0^4}{r^4} \right) \sin 2\theta \end{cases} \quad (12)$$

The expression of abutment pressure can be obtained by bringing Equation (13) into Equation (7), and then the coordinate transformation of the three stress components caused by abutment pressure in the floor rock layer can be obtained. The expressions of radial stress σ_{r2} , circumferential stress $\sigma_{\theta2}$ and tangential stress $\tau_{r\theta2}$ caused by abutment stress in the polar coordinate system shown in Figure 14.

$$\begin{cases} x = x' + r \cos \theta \\ z = z' + r \sin \theta \end{cases} \quad (13)$$

$$\begin{cases} \sigma_{r2} = \frac{\sigma'_x + \sigma'_z}{2} + \frac{\sigma'_x - \sigma'_z}{2} \cos 2\theta - \tau'_{xz} \sin 2\theta \\ \sigma_{\theta2} = \frac{\sigma'_x + \sigma'_z}{2} - \frac{\sigma'_x - \sigma'_z}{2} \cos 2\theta + \tau'_{xz} \sin 2\theta \\ \tau_{r\theta2} = \frac{\sigma'_x - \sigma'_z}{2} \sin 2\theta + \tau'_{xz} \cos 2\theta \end{cases} \quad (14)$$

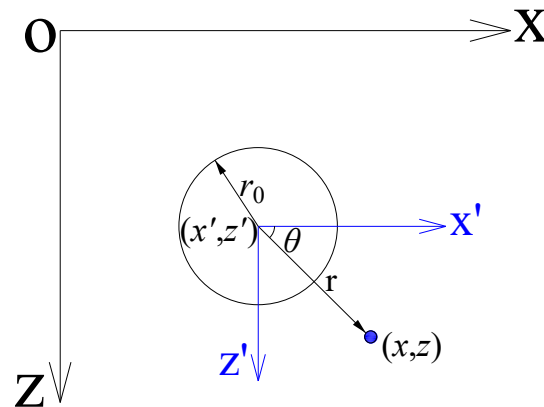


Figure 14. Coordinate transformation diagram.

According to the above analysis, the stress expression of the surrounding rock of the floor roadway under mining stress can be obtained by adding Formulas (12) and (14).

$$\begin{cases} \sigma_r = \sigma_{r1} + \sigma_{r2} \\ \sigma_\theta = \sigma_{\theta1} + \sigma_{\theta2} \\ \tau_{r\theta} = \tau_{r\theta1} + \tau_{r\theta2} \end{cases} \quad (15)$$

Using Matlab and origin to draw the circumferential stress and radial stress cloud diagram of roadway surrounding rock under different coal pillar widths, as shown in Figure 15.

The width of the coal pillar for roadway protection in Qinan Coal Mine was originally designed to be 80 m. In the process of reducing the width of the coal pillar from 80 m to 30 m, the peak values of circumferential stress and radial stress of the surrounding rock of the roadway increased continuously. Under the action of radial stress, the risk of the roof and floor of the roadway being compressed and moved closer is increasing. Under the action of circumferential stress, the risk of 'bulging' of the two sides of the roadway is gradually increasing. In addition, because the stress concentration of the surrounding rock on the left side of the roadway is slightly greater than that on the right side, the deformation risk on the left side of the roadway is also slightly greater than that on the right side. When the width of the coal pillar decreases from 30 m to 0 m, the roadway is located below the influence range of advance abutment pressure of the coal seam. The surrounding rock of the roadway is most affected by mining stress, and the concentration degree of circumferential stress and radial stress is more significant. Under the action of deviatoric stress, the risk of 'shrinkage' in the upper right of the roadway is greater, and the risk of 'bulging' in the lower right of the roadway is greater. Overall, the deformation risk on the right side of the roadway is greater than that on the left side. When the roadway is located below the goaf, the peak circumferential stress and radial stress of the surrounding rock of the roadway are reduced to below the peak stress of the static pressure roadway, and the deformation risk of the surrounding rock of the roadway is reduced. When the coal pillar width is -30 m, the roadway is located below the goaf, and the circumferential stress and radial stress distribution of the surrounding rock of the roadway are more complicated. However, the peak circumferential stress and the peak radial stress are smaller than the peak circumferential stress and the peak radial stress of the surrounding rock of the static pressure roadway, and the surrounding rock of the roadway is in a state of pressure relief.

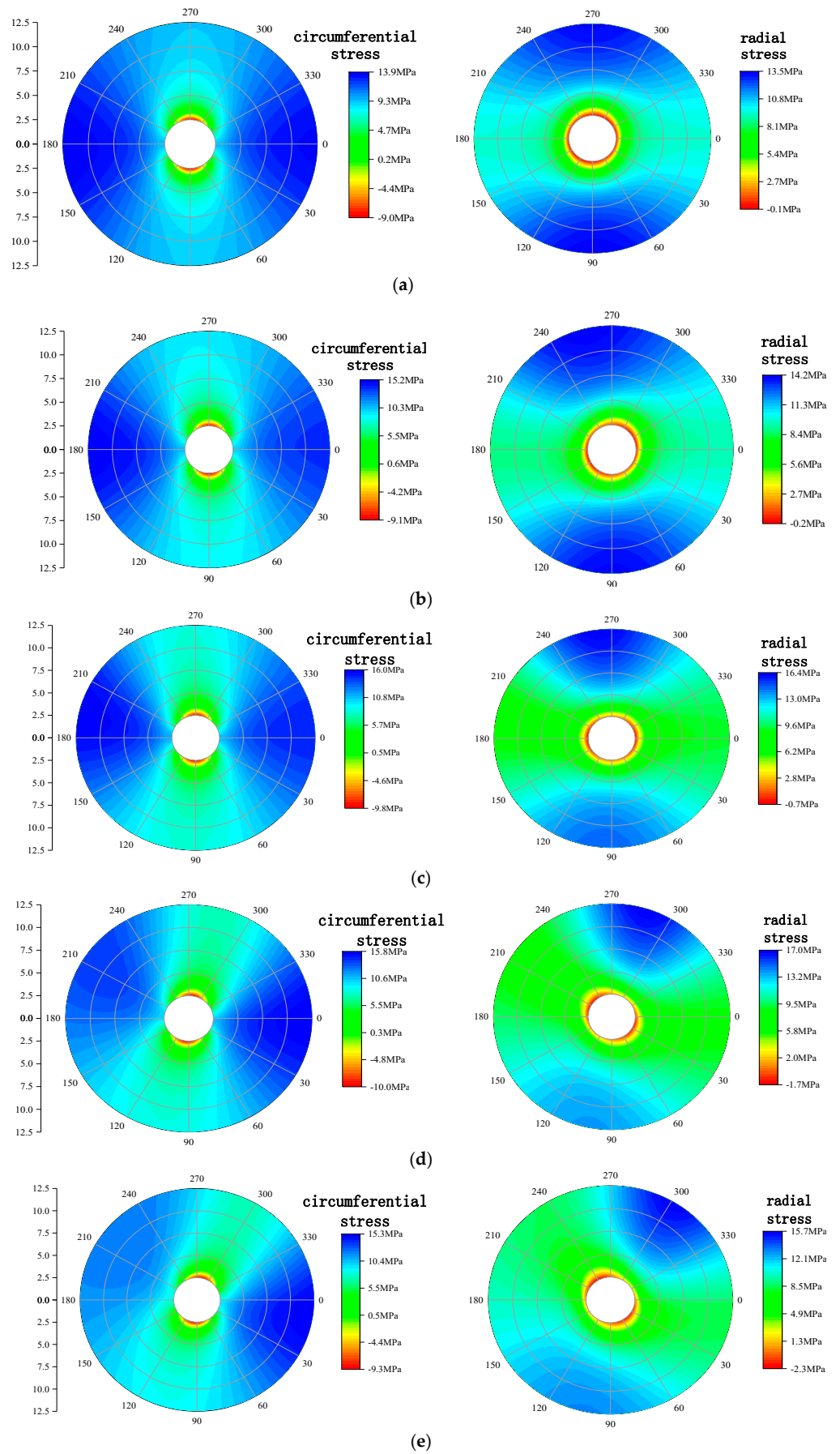


Figure 15. Cont.

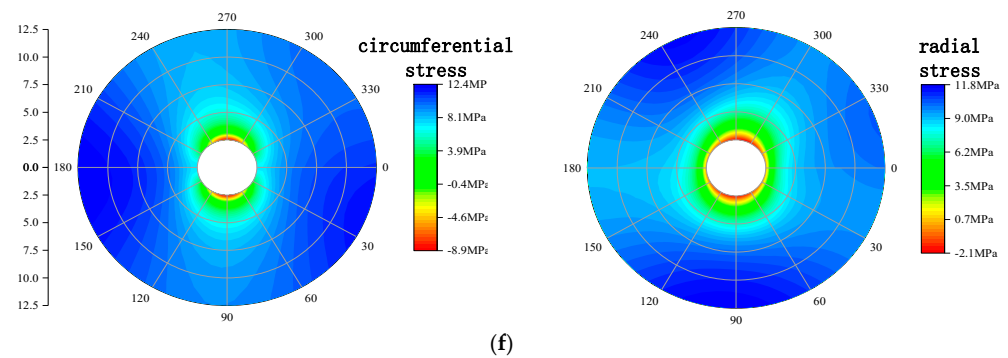


Figure 15. Circumferential stress and radial stress of surrounding rock of roadway with different coal pillar widths: (a) The width of coal pillar is 80 m; (b) The width of coal pillar is 50 m; (c) The width of coal pillar is 30 m; (d) The width of coal pillar is 10 m; (e) The width of coal pillar is 0 m; (f) The width of coal pillar is −30 m (the working face crosses the floor roadway 30 m).

According to the elastic mechanics, the expressions of the maximum principal stress σ_{h1} and the minimum principal stress σ_{h2} of the roadway surrounding rock in the X-Z plane are

$$\begin{cases} \sigma_{h1} = \frac{\sigma_r + \sigma_\theta}{2} + \sqrt{\left(\frac{\sigma_r - \sigma_\theta}{2}\right)^2 + \tau_{r\theta}^2} \\ \sigma_{h2} = \frac{\sigma_r + \sigma_\theta}{2} - \sqrt{\left(\frac{\sigma_r - \sigma_\theta}{2}\right)^2 + \tau_{r\theta}^2} \end{cases} \quad (16)$$

Therefore, the expressions of the maximum principal stress σ'_1 , the intermediate principal stress σ'_2 , the minimum principal stress σ'_3 under the action of three-dimensional stress in the surrounding rock of the roadway are as follows:

$$\begin{cases} \sigma'_1 = \max(\sigma_y, \sigma_{h1}) \\ \sigma'_2 = \min(\sigma_y, \sigma_{h1}) \\ \sigma'_3 = \sigma_{h2} \end{cases} \quad (17)$$

According to the Mohr-Coulomb strength criterion, the rock mass state function of the roadway's surrounding rock is established.

$$f_h = \sigma'_1 - \frac{1 + \sin\varphi_h}{1 - \sin\varphi_h} \sigma'_3 - \frac{2C_h \cos\varphi_h}{1 - \sin\varphi_h} \quad (18)$$

The floor roadway is located in the sandstone layer. Due to the disturbance of the roadway to the surrounding rock mass, the mechanical parameters of the surrounding rock mass of the roadway are significantly reduced compared with the undisturbed sandstone layer rock mass. According to the Hoek-Brown strength criterion, the rock mass parameters of 'sandstone-2' without disturbance in Table 2 are transformed into the solution of rock mass parameters under disturbance, and the rock mass parameters of roadway surrounding rock can be obtained, as shown in Table 2.

Table 2. Parameters of surrounding rock mass of floor roadway.

| Rock | Density/Kg·m ⁻³ | Elastic Modulus/GPa | Poisson Ratio | Cohesion/MPa | Angle of Internal Friction/° | Tensile Strength/MPa |
|------------------|----------------------------|---------------------|---------------|--------------|------------------------------|----------------------|
| Surrounding rock | 2590 | 4.33 | 0.16 | 3.29 | 30.86 | 1.92 |

According to Formula (18), the failure risk area of the surrounding rock of the roadway under the coal pillar width of 80 m, 50 m, 30 m, 10 m, 0 m, and −30 m is obtained, as

shown in Figure 16. It can be seen from the figure that when the width of the coal pillar is 30 m, the depth of the 'rectangular four corners' of the failure zone is the largest, and the maximum depth is about 1.8 m. When the width of the coal wall is reduced from 30 m to 10 m, the failure zone of the surrounding rock develops rapidly, especially the upper left of the roadway roof and the lower right of the floor. The shape of the failure zone is approximately parallelogram, and the maximum failure depth is more than 2 m. When the width of the coal pillar is less than 10 m, the range of the failure zone begins to decrease gradually, and the degree of danger decreases gradually. When the width of the coal pillar is 0 m, the shape of the failure risk zone is similar to that of the coal pillar width of 10 m, but the range of the failure risk zone is reduced. As the working face continues to move forward, the range of the failure risk zone of the roadway's surrounding rock gradually decreases, and the shape of the failure risk zone gradually recovers from parallelogram to rectangle. When the width of the coal pillar is equal to -30 m, the range of the failure risk zone basically recovers to the range of the failure zone before the width of the coal pillar is 30 m.

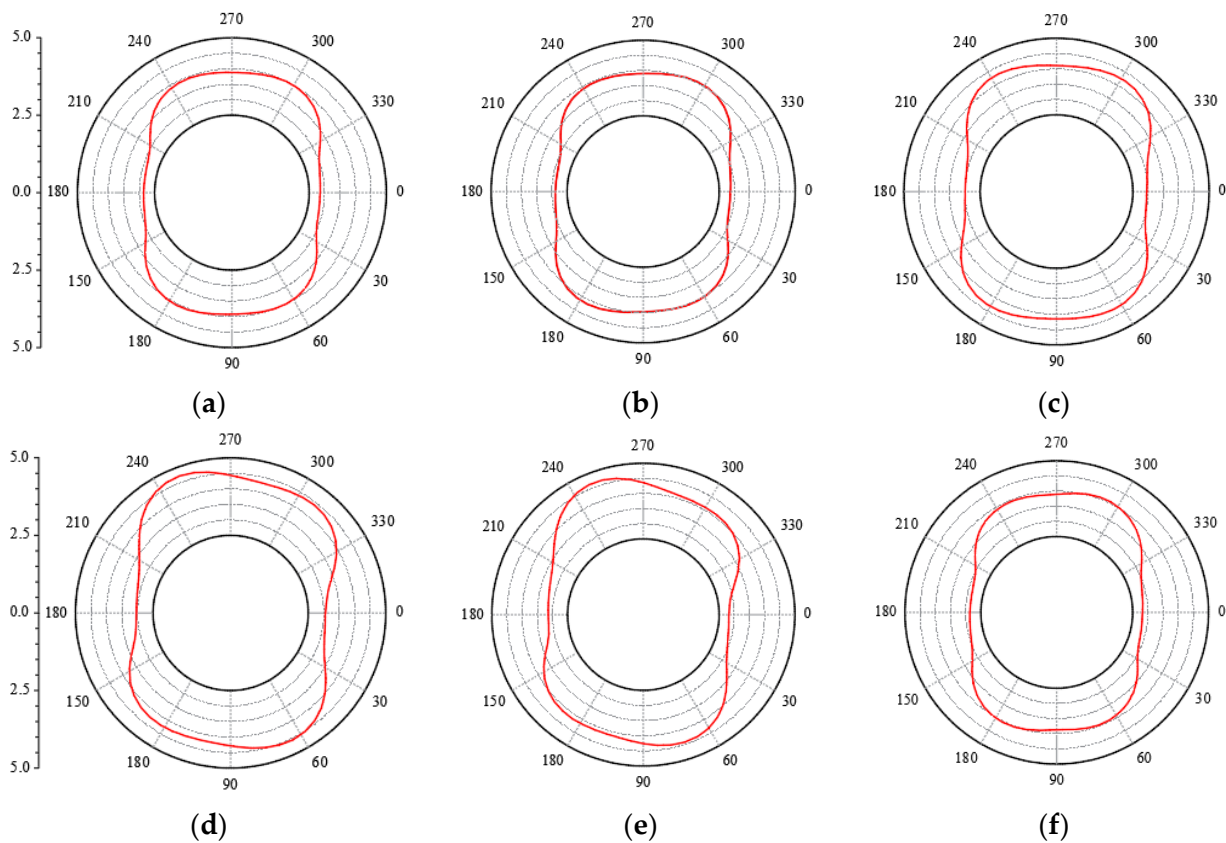


Figure 16. Risk area of roadway surrounding rock failure under different coal pillar widths: (a) Coal pillar width of 80 m; (b) Coal pillar width of 50 m; (c) Coal pillar width of 30 m; (d) Coal pillar width of 10 m; (e) Coal pillar width of 0 m; (f) Coal pillar width of -30 m (the working face crosses the floor roadway 30 m).

4.2. Numerical Calculation and Analysis of Surrounding Rock Stability of the Floor Roadway under the Influence of Mining Stress

4.2.1. Model Set-Up

According to the position relationship between the 313 working face of Qinan Coal Mine and the east wing rail transportation roadway, based on the numerical calculation model of the floor strata in the third chapter, a three-dimensional numerical calculation model of the surrounding rock of the cross mining floor roadway is established. The size of the surrounding rock of the roadway is $16 \times 204 \times 16$ m, the floor of the roadway is

40 m away from the floor of the upper working face, the X coordinate of the center of the roadway is 300 m, and the Z coordinate is -38.5 m.

After the model is established, the roadway is filled first, and the roadway is excavated when the model reaches equilibrium. After the excavation, the model is restored to the equilibrium state again. Finally, the coal seam mining is simulated, and the evolution law of the stress field and the failure zone of the surrounding rock of the floor roadway during the cross-mining process is analyzed.

4.2.2. Vertical Stress Distribution Characteristics of Roadway Surrounding Rock

In the process of cross-mining, with the decrease in coal pillar width, the change in vertical stress peak on both sides of the roadway is shown in Figure 17.

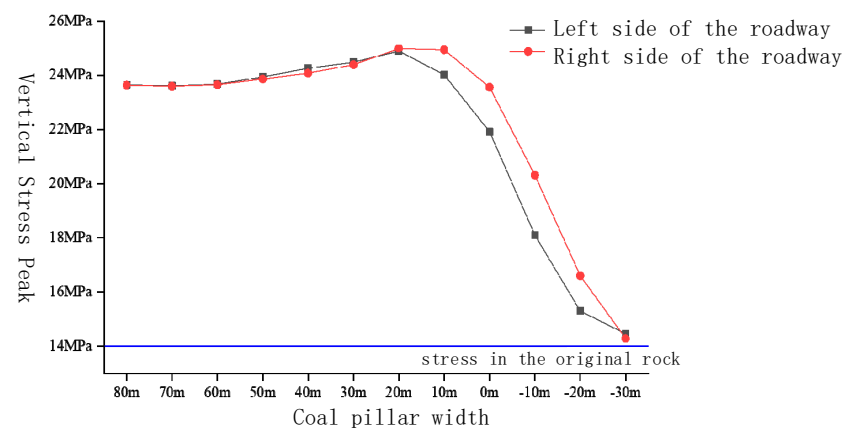


Figure 17. Peak vertical stress on both sides of the roadway under different coal pillar widths.

When the coal pillar width is greater than 60 m, the vertical stress peaks on both sides of the roadway are basically equal, and the vertical stress peaks on both sides have not changed significantly. When the width of the coal pillar is less than 60 m, the influence of mining stress on the surrounding rock of the floor roadway gradually appears. The vertical stress concentration on the left side of the roadway is greater than that on the right side of the roadway when the width of the coal pillar decreases from 60 m to 30 m and reaches the maximum when the width of the coal pillar is equal to 20 m. The vertical stress concentration on the right side of the roadway is greater than that on the left side of the roadway when the width of the coal pillar is less than 20 m and reaches the maximum in the range of 20–10 m. When the working face crosses the floor roadway, the vertical stress peak of the surrounding rock on both sides of the roadway decreases rapidly. When the working face passes through the floor roadway for 30 m, the vertical stress peak of the surrounding rock on both sides of the roadway basically recovers to the original rock stress, and the surrounding rock of the roadway is in the stress reduction area as a whole. The results are basically consistent with the theoretical analysis.

4.2.3. Analysis of the Scope of Surrounding Rock Failure Zone of Floor Roadway

This section analyzes the distribution characteristics and evolution law of the failure zone of the surrounding rock of the roadway during the cross-mining process by studying the damage degree of the surrounding rock of the floor roadway under different coal pillar widths. Figure 18 is the distribution map of the failure zone of the roadway's surrounding rock in different stages of cross-mining.

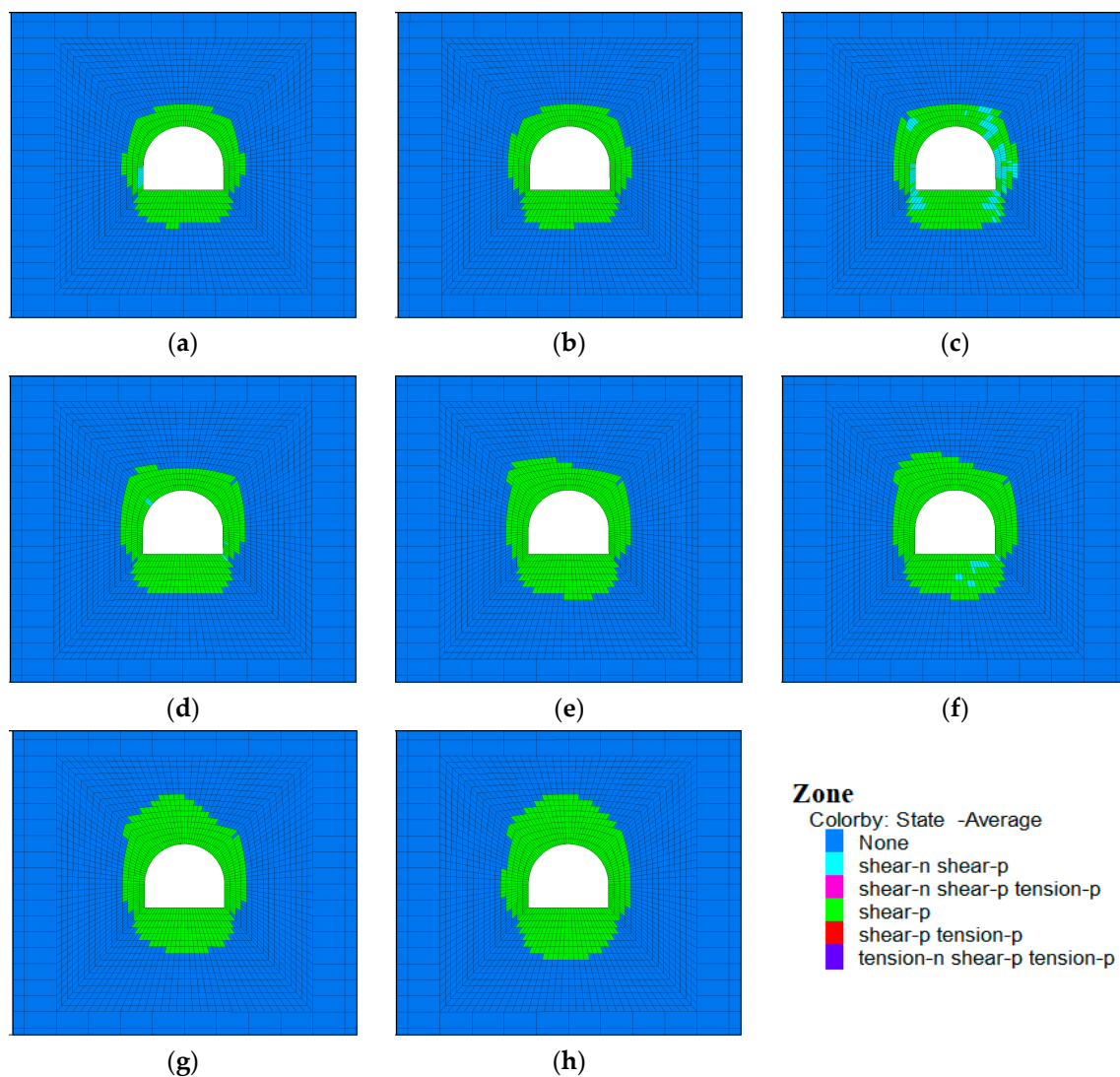


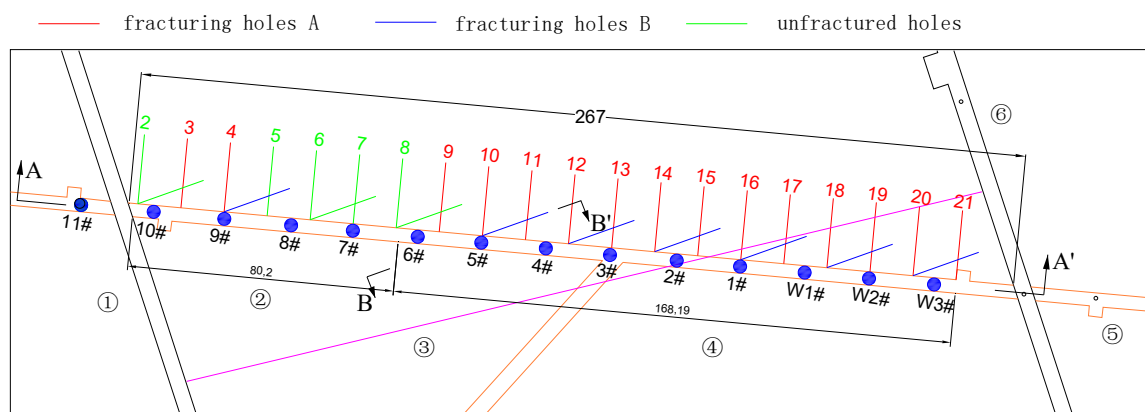
Figure 18. Evolution of the damaged area across the mining floor roadway: (a) Coal pillar width of 80 m; (b) Coal pillar width of 40 m; (c) Coal pillar width of 30 m; (d) Coal pillar width of 20 m; (e) Coal pillar width of 10 m; (f) Coal pillar width of 0 m; (g) Coal pillar width of -10 m (h) Coal pillar width of -30 m (the working face crosses the floor roadway 30 m).

According to the analysis of the simulation effect diagram 3.6, when the width of the coal pillar is 80 m, the failure zones on the left and right sides of the surrounding rock of the floor roadway are basically symmetrical. The maximum failure depth of the surrounding rock of the roadway floor is more than 2.4 m, and the failure zone of the left surrounding rock is slightly larger than that of the right side. In the process of reducing the width of the coal pillar from 80 m to 30 m, the failure zone of the roadway roof mainly develops to the right side, the failure zone of the roadway floor mainly develops to the left side, and the development speed of the failure zone of surrounding rock in the left side of the roadway is greater than that in the right side. When the coal pillar width decreases from 30 m to 0 m, the roof failure zone mainly develops to the left side, the floor failure zone mainly develops to the right side, and the range of the two side failure zones does not change much. In the process of reducing the width of the coal pillar from 0 m to -30 m, the failure zone of the roadway roof still maintains a rapid development speed and develops to the deep part of the surrounding rock in the upper left. As the working face continues to move forward, the influence of advance abutment pressure on the floor roadway is getting smaller and smaller, the failure depth of the roof is basically unchanged, and the failure zone develops

to the right side. The floor failure zone develops to the left and develops to the deep at the same time as the failure zone of the surrounding rock on the two sides.

5. Engineering Practice

Based on the above analysis results, the hydraulic fracturing implementation plan of the East Wing Rail Transit Lane is determined as shown in Figure 19. Fracturing boreholes are drilled in the East Wing Rail Transit Lane for hydraulic fracturing. The length of the main roadway below the working face is 267 m, the fracturing section is 169 m, and the non-fracturing section is 98 m. Drilling A is constructed in the inclined roof strata of the vertical roadway, with an elevation angle of 45° . Borehole B is constructed with an angle between the direction of the main roadway, with an azimuth angle of 25° , an elevation angle of 45° , a borehole diameter of 94 mm, a spacing of 13 m, and a length of 30 m. Fracturing starts from the bottom of the hole, and fracturing is performed once every 3 m back. Each borehole is fractured in 5 sections, and the fracturing time of each section is controlled at 25–30 min.



①313haulage roadway ②unfractured section ③predicted stop line
④fractured section ⑤east wing rail transport alley ⑥313return airway

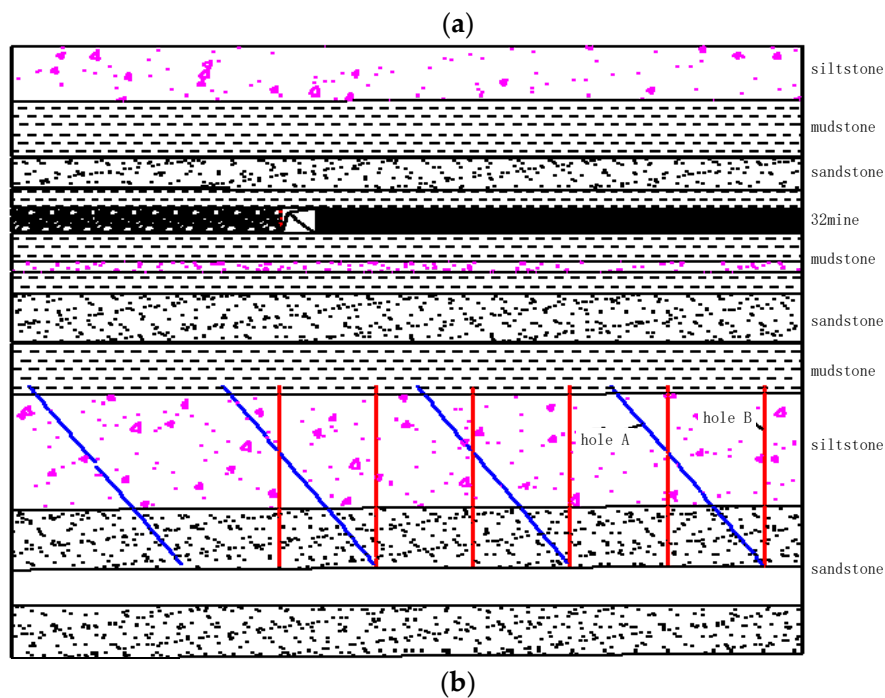


Figure 19. Cont.

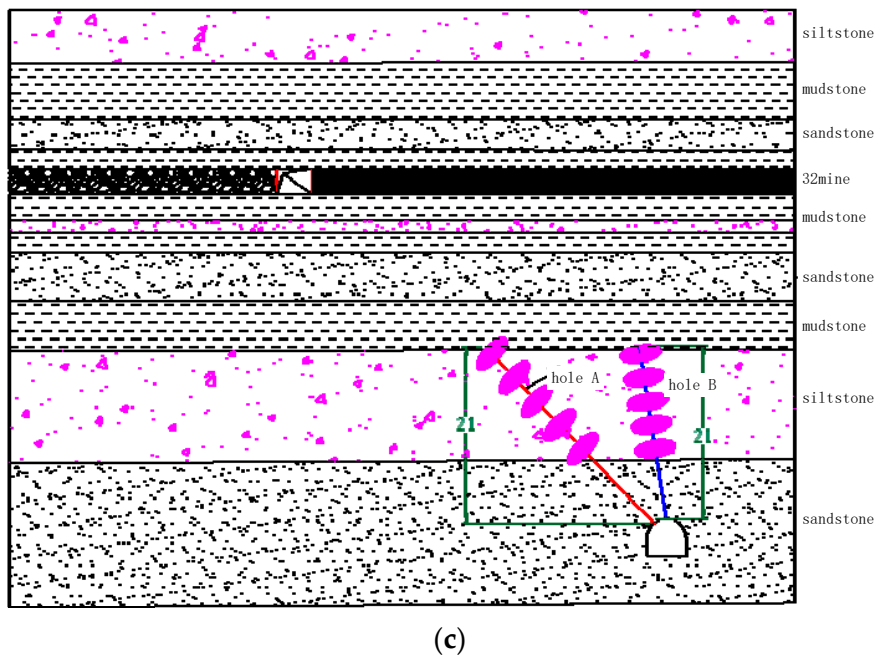


Figure 19. Hydraulic fracturing borehole layout of east wing rail transport roadway: (a) plane figure; (b) A-A' profile diagram; (c) B-B' profile diagram.

Because the roadway intersects with the working face space, in order to evaluate the application effect of hydraulic fracturing, the intersection point of the unfractured side is set as the 0 point position of the roadway, and the roadway deformation monitoring points are set at 17.5 m, 1 m, -4.5 m, -6 m, -12 m, -17 m, -23 m, -31 m, -41 m, -45.5 m, -51.5 m, and -57.5 m from the working face in the roadway. The deformation of the roadway in the fractured and non-fractured sections is shown in Figure 20. The maximum displacement of the roof and floor of the unfractured section is 370 mm, and the maximum displacement of the two sides is 230 mm. The maximum displacement of the roof and floor of the fracturing section is 85 mm, and the maximum displacement of the two sides is 60 mm. After fracturing, the roof-to-floor convergence is reduced by 77%, and the two-side convergence is reduced by 74%.

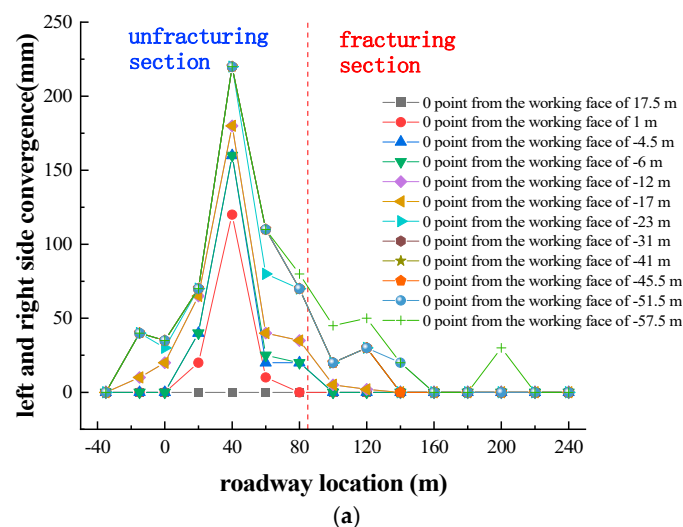


Figure 20. Cont.

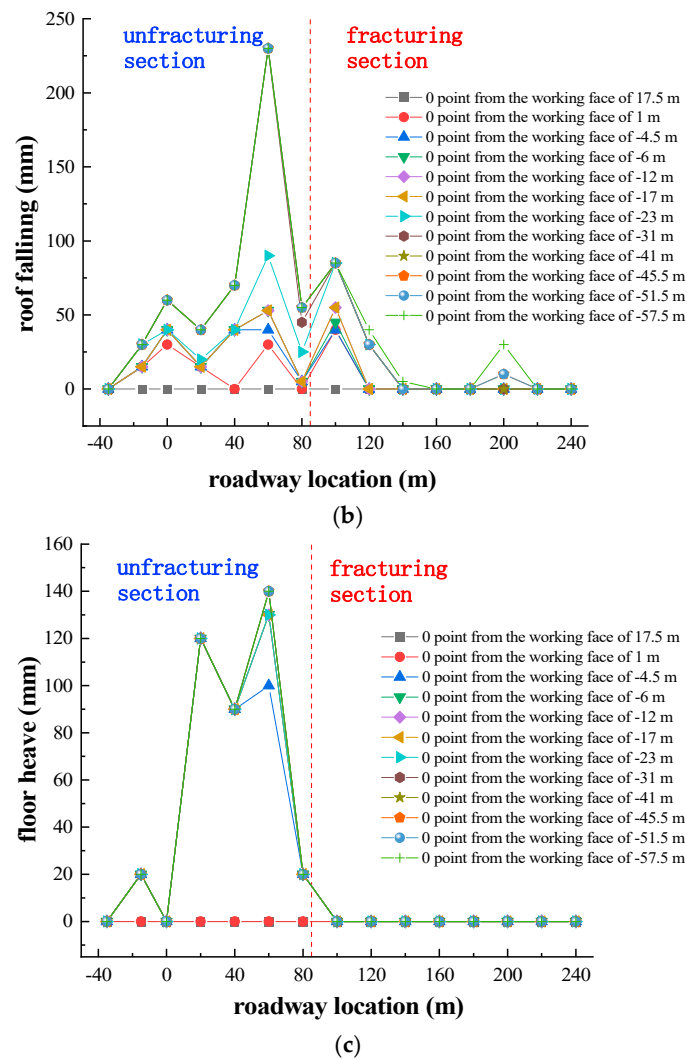


Figure 20. Deformation of roadway in fracturing section and non-fracturing section: (a) The amount of left and right side convergence; (b) roof falling capacity; (c) floor heave amount.

The shape of the roadway in the hydraulic fracturing section and the unfractured section is shown in Figure 21. It can be seen that the roof of the roadway in the non-fractured section is relatively broken, and the roof subsidence and floor heave are obvious. The deformation of the surrounding rock of the roadway is obviously small, the roof integrity is good, and the roadway is effectively controlled.



Figure 21. Roadway shape with or without fracturing and pressure relief: (a) unfractured section; (b) fracturing section.

6. Conclusions

This paper's research combines on-site research, theoretical analysis, and numerical simulation to more comprehensively analyze and study the stress field and damage zone evolution law of the bottom roadway peripheral rock in the process of trans-mining and puts forward the hydraulic fracturing decompression scheme. The deformation of the roadway's peripheral rock is effectively controlled, which is of certain guiding significance for the maintenance and sustainable use of the bottom roadway and better guarantees the sustainable exploitation of the coal in the wells. The main conclusions are as follows.

(1) The propagation law of mining-induced stress in the floor strata is studied. The influence of mining-induced stress on the vertical stress of the floor strata is mainly reflected in the stress-increasing area in front of the coal wall. The main body behind the coal wall is mainly the stress reduction zone. With the increase in the depth of the floor rock layer, the peak value of the vertical stress gradually decreases, and the distance from the peak value of the vertical stress to the coal wall and the influence range of the vertical stress gradually increase.

(2) With the advance of the cross-mining working face, the stress concentration degree and the range of the high-stress area of the surrounding rock of the floor roadway increase obviously within the influence range of the abutment pressure of the working face. When the working face crosses the floor roadway, the stress concentration degree and the range of the high-stress area of the roadway's surrounding rock decrease rapidly. The high-stress area in front of the working face is connected with the high-stress area of the surrounding rock on the left side of the roadway, which is an important reason for the deformation of the surrounding rock of the floor roadway.

(3) The evolution characteristics of the plastic zone of surrounding rock in the floor roadway are analyzed. When the width of the coal pillar is greater than the influence range of advance abutment pressure of the working face, the development speed of the plastic zone is slow. When the roadway is located in the influence range of advance abutment pressure, the plastic zone of the roadway's surrounding rock develops rapidly. When the working face crosses the floor roadway more than 10 m, the maximum depth of the plastic zone of the surrounding rock of the roadway is no longer increased.

(4) By analyzing the failure law of the floor strata of the working face under mining stress and the stress evolution characteristics of the surrounding rock of the roadway during the cross-mining process, it is determined that the time of hydraulic fracturing should be before the width of the coal pillar is greater than 40 m, and the fracturing layer is the main bearing layer sandstone layer above the roadway.

(5) The field industrial test shows that the maximum displacement of the roof and floor in the non-fracturing section is 370 mm, the maximum displacement of the two sides is 230 mm, the maximum displacement of the roof and floor in the fracturing section is 85 mm, the maximum displacement of the two sides is 60 mm, the displacement of the roof and floor is reduced by 77%, the displacement of the two sides is reduced by 74%, and the deformation of the surrounding rock of the cross mining floor roadway is effectively controlled.

Author Contributions: Y.C. and H.L.; Data curation: C.L.; Formal analysis: Y.C., H.L. and S.L.; Funding acquisition: C.L.; Methodology: C.L. and H.L.; Writing—original draft: Y.C., H.L. and S.L.; Writing—review and editing: Y.C. and S.L. All authors have read and agreed to the published version of the manuscript.

Funding: This study is supported by National Natural Science Foundation of China (52074267).

Institutional Review Board Statement: The Institutional Review Board (IRB) has carefully reviewed the proposed research project and determined that it meets all ethical and regulatory requirements. The IRB has ensured that the rights and welfare of all participants are protected, and that the research design and methods are scientifically sound and appropriate. Additionally, the IRB has approved the informed consent procedures and the data collection and management plans. The IRB will continue to monitor the progress of the research and ensure that any changes to the protocol are appropriately reviewed and approved. The IRB is committed to promoting ethical conduct in research and safeguarding the interests of all involved.

Informed Consent Statement: Informed consent was obtained from all subjects involved in the study.

Data Availability Statement: The data that support the findings of this study are available from the corresponding author, [Yiqi Chen], upon reasonable request.

Acknowledgments: We would like to thank the mining engineers and workers for their help in field surveys and industrial tests.

Conflicts of Interest: The authors declare no conflicts of interest.

References

- Kang, H.P.; Zhang, X.; Wang, D.P.; Tian, J.Z.; Yi, Z.Y.; Jiang, W. Surrounding rock control technology and application of non-pillar mining. *J. China Coal Soc.* **2022**, *47*, 16–44. [\[CrossRef\]](#)
- Zhang, H.L.; Wang, L.G. Study on calculation and application of additional stress of mining floor. *J. Min. Saf. Eng.* **2011**, *28*, 288–292, 297.
- Feng, L.; Zhao, G.M.; Meng, X.R. Analytical method calculation and application of floor failure law of coal mining above confined water. *Coal Sci. Technol.* **2011**, *39*, 13–16. [\[CrossRef\]](#)
- Huang, Q.S.; Cheng, J.L. Study on analytical calculation model of mining-induced stress field of layered floor. *J. Min. Sci.* **2017**, *2*, 559–565. [\[CrossRef\]](#)
- Ti, Z.Y.; Li, J.Z.; Wang, M.; Zhu, Z.J.; Zhang, F.; Hu, J.T. Study on mining failure depth of inclined coal seam floor based on fracture mechanics. *J. Cent. China Norm. Univ. (Nat. Sci.)* **2020**, *54*, 787–791, 797.
- Zhu, L.; Liu, C.Y.; Gu, W.Z.; Yuan, C.F.; Wu, Y.Y.; Liu, Z.C.; Song, T.Q.; Sheng, F.T. Research on Floor Heave Mechanisms and Control Technology for Deep Dynamic Pressure Roadways. *Processes* **2023**, *11*, 467. [\[CrossRef\]](#)
- Wilson, A.H. The stability of underground workings in the soft rocks of the Coal Measures. *Int. J. Min. Eng.* **1983**, *1*, 91–181. [\[CrossRef\]](#)
- Zhai, X.X.; Jiang, X.Y.; Qian, M.G.; Du, J.P.; Lu, X.Y.; Zhang, S.Y.; Yu, Y.X.; Li, H.M. Relationship between surrounding rock deformation and mining depth of floor roadway under moving pressure support. *J. Jiaozuo Min. Coll.* **1994**, *13*, 16–20.
- Wang, P.P.; Zhao, Y.X.; Jiang, Y.D.; Zhang, C.; Zhang, D.Y.; Yang, J.H.; Liu, W.C.; Zhai, J.P. Floor water inrush characteristics and control technology of deep mining under pressure in Xingdong Mine. *J. China Coal Soc.* **2020**, *45*, 2444–2454.
- He, F.L.; Zhai, W.L.; Xu, X.H.; Song, J.Y.; Li, L.; Lv, K. Study on Mechanism and Control Technology of Asymmetric Floor Heave in a Deep Soft Rock Main Roadway. *Geofluids* **2022**, *2022*, 1149000. [\[CrossRef\]](#)
- Liu, W.T.; Mu, D.R.; Xie, X.X.; Zhang, W.; Yuan, D.L. Mining stress distribution law and failure characteristics of inclined coal seam floor. *J. Min. Saf. Eng.* **2018**, *35*, 756–764.
- Skrzypkowski, K.; Zagórski, K.; Zagórska, A.; Apel, D.B.; Wang, J.; Xu, H.; Guo, L. Choice of the Arch Yielding Support for the Preparatory Roadway Located near the Fault. *Energies* **2022**, *15*, 3774. [\[CrossRef\]](#)
- Li, X.H.; Yao, Q.L.; Zhang, N.; Wang, D.Y.; Zheng, X.G.; Ding, X.L. Simulation Study on Stability of Surrounding Rock in High Level Stress Cross Mining Roadway. *J. Min. Saf. Eng.* **2008**, *25*, 420–425.
- Li, G.C.; Ma, Z.Q.; Zhang, N.; Wang, P.P.; Ma, R. Study on failure characteristics and control countermeasures of multiple cross-mining roadways in Huaibei mining area. *J. Min. Saf. Eng.* **2013**, *30*, 181–187.
- Chen, S.Y.; Song, C.S.; Guo, Z.B.; Wang, J.; Wang, Y. Mechanical mechanism and control countermeasures of asymmetric deformation of deep dynamic pressure roadway. *J. China Coal Soc.* **2016**, *41*, 246–254. [\[CrossRef\]](#)
- Chen, J.X. Prestressed bolt support technology of floor rock roadway under complex conditions in deep mine. *Coal Sci. Technol.* **2006**, *34*, 22–24. [\[CrossRef\]](#)
- Zhou, X.M.; Wang, S.; Li, X.L.; Meng, J.J.; Li, Z.; Zhang, L.H.; Pu, D.D.; Wang, L.K. Research on Theory and Technology of Floor Heave Control in Semicool Rock Roadway: Taking Longhu Coal Mine in Qitaihe Mining Area as an Example. *Lithosphere* **2022**, *2022*, 3810988. [\[CrossRef\]](#)
- Zhao, Q.F.; Wang Bo Zheng, S.D.; Shi, J.J.; Liu, Y.Y. Surrounding rock failure characteristics and pressure relief control technology of mining floor roadway in upper coal seam. *Coal Eng.* **2016**, *48*, 77–80.
- Wang, T.J.; Tian, C.D. Insufficient mining cross-uphill test in deep mine working face. *Ground Press. Strat. Control.* **2000**, 10–11+14.
- Qiang, M.G.; Shi, P.W.; Xu, J.L. *Ground Pressure and Strata Control. 2*; China University of Mining and Technology Press: Xuzhou, China, 2010. [\[CrossRef\]](#)

21. Xu, Z.L. *Elastic Mechanics Brief Tutorial. 5*; Higher Education Press: Beijing, China, 2018.
22. Du, Z.S. *Study on Deformation Mechanism of Surrounding Rock of Floor Roadway in Slope Based on In-Situ Stress-Sedimentary Rock Layer Structure Control*; Anhui University of Science and Technology: Huainan, China, 2017.

Disclaimer/Publisher's Note: The statements, opinions and data contained in all publications are solely those of the individual author(s) and contributor(s) and not of MDPI and/or the editor(s). MDPI and/or the editor(s) disclaim responsibility for any injury to people or property resulting from any ideas, methods, instructions or products referred to in the content.